

Article

Dynamic Concentrated Solar Building Skin Design Based on Multiobjective Optimization

Zebiao Shao , Bo Wang , Yao Xu, Liang Sun, Xichen Ge, Lvpei Cai and Cheng Chang

School of Architecture and Design, China University of Mining and Technology, Xuzhou 221116, China

* Correspondence: ts20190037p31@cumt.edu.cn; Tel.: +86-180-2055-3667

Abstract: Building skin can provide comprehensive functions of energy production, daylighting, and shading with an integrated transmissive solar-concentrating panel. In this study, Rhino Grasshopper parametric modeling, Ladybug tool performance simulation, and Octopus multiobjective optimization platforms are used to carry out experimental research. This study establishes the optimal relationship between the conflicting objectives of light environment creation and energy production efficiency of solar-concentrating skin by controlling three variables, namely the size of the solar-concentrating module, the rotation angle, and the number of modules, aiming to design the optimal solution and build a multiobjective optimization technology framework for the solar-concentrating skin of an office space. A comparison and analysis of the scenarios indicate a dynamic concentrating skin that can effectively reduce the daylight glare probability (DGP) by 70% and increase the useful daylight illuminance (UDI) by 10%, while achieving energy production. The correlation between the variables and the performance indices of the solar-concentrating skin was obtained as angle > width > length > amount, and the optimal design interval for each parameter variable. This study reveals the laws of how parameter changes affect individual indicators, which can provide ideas for the design of dynamic concentrating skins and building integration, methods for improving the balanced design of indoor light environments and building capacity, and a technical framework for multiobjective optimization processes.

Keywords: dynamic solar-concentrating skin; indoor light environment; performance optimization; energy efficiency; daylighting quality; Pareto optimal



Citation: Shao, Z.; Wang, B.; Xu, Y.; Sun, L.; Ge, X.; Cai, L.; Chang, C. Dynamic Concentrated Solar Building Skin Design Based on Multiobjective Optimization. *Buildings* **2022**, *12*, 2026. <https://doi.org/10.3390/buildings12112026>

Academic Editor: Antonio Caggiano

Received: 21 October 2022

Accepted: 16 November 2022

Published: 18 November 2022

Publisher's Note: MDPI stays neutral with regard to jurisdictional claims in published maps and institutional affiliations.



Copyright: © 2022 by the authors. Licensee MDPI, Basel, Switzerland. This article is an open access article distributed under the terms and conditions of the Creative Commons Attribution (CC BY) license (<https://creativecommons.org/licenses/by/4.0/>).

1. Introduction

According to the Global Building Construction Status Report 2021, the construction field accounted for 37% of energy-related CO₂ emissions in 2020 [1]. In the context of global advocacy for reducing carbon emissions, the construction field needs to change existing building energy efficiency policy standards and realize better energy-saving technologies to achieve a real transformation of the construction industry in order to cope with increasing carbon emissions. Using renewable energy to develop energy-efficient buildings to reduce energy consumption and carbon emissions is an important way to reduce carbon emissions and achieve green and sustainable development.

Building-integrated photovoltaics (BIPV) are widely used in this context and serve the purpose of saving energy and reducing carbon emissions. However, their traditional single form, integrated location, and uniform specifications limit the expression of the building facade form; this form is more monotonous after being integrated with the facade of the building, leading to its low application and acceptance [2]. Compared to integration on the roof of the building and integration of PV modules into the building curtain walls, windows, and other transparent parts, opaque modules will have an impact on the natural lighting of the building, resulting in problems such as insufficient illumination at the location of a large internal depth of the building, poor lighting uniformity, and annual daylight illumination in the effective range of the working time period, which does not meet

the requirements. The semitransparent form of photovoltaic modules integrated with the building, to a certain extent, takes into account the natural lighting of the building, as well as the indoor light environment and photovoltaic conversion efficiency [3,4]. These lighting problems can lead to poor indoor light environment comfort, increased dependence on artificial lighting, and increased energy consumption [5]. Related studies have found that lighting energy consumption in office buildings accounts for 20–40% of the total building energy consumption [6].

With the continuous development of photovoltaic technology, the integration of building-integrated concentrating photovoltaic (BICPV) modules in buildings will bring about changes in the building skin form, indoor natural light environment, and building energy systems. The solar-concentrating module only absorbs direct light for energy production during operation, and the scattered light can enter the room for lighting through the solar-concentrating module [7], which realizes the cascading utilization of natural light, reduces the indoor light environment problems caused by excessive direct light, and creates a good indoor light environment [8,9]. Compared to BIPV, BICPV has a higher energy yield efficiency [10,11], which enables dynamic shading when tracking light production capacity and improves users' perception of indoor environmental changes. A research team at the Rensselaer Polytechnic Institute designed and implemented a BICPV façade system, which also demonstrated that BICPV can collect solar energy to produce energy while still providing indoor diffuse daylight and outdoor view to users, as well as significantly improve indoor glare and enhance user perception [12,13].

The relationship between BICPV and building skin morphology, natural lighting, and energy production has contributed to the beginning of continuous research on BICPV by domestic and international scholars. Chemisana [14] and Maghrabie et al. [15] investigated the suitability of a BICPV integrated design. Parupudi et al. [16] studied building-integrated low-frequency concentrated solar energy utilization and optimized the design of the geometry of the solar-concentrating unit. Baig et al. [17] and Zhu et al. [7] quantified the optical performance of the system under different conditions by designing a novel BICPV system. Hong et al. [18] proposed a new transmissive solar-concentrating system for glass curtain wall integration.

Xuan et al. [19,20] designed asymmetric concentrated photovoltaic windows suitable for building south walls, and new BICPV windows. Zhang et al. [21] designed a low-frequency transmissive solar-concentrating module for light window integration, and all proved through simulation and experimental studies that the integration of the novel concentrating system on the building can comfortably meet the indoor lighting requirements of the building.

Most of the domestic and international studies are biased toward the module design [12,13,16], integration design [14,15], optical transmission characteristics [7,17], and the impact on the indoor light environment [18,21] of the solar-concentrating system; however, there are few comprehensive studies on the energy output, indoor light environment, indoor and outdoor views, and other demanded objectives after the integration of the solar-concentrating module with the building, mostly using experimental and simulation types of research methods.

If BICPV is to be better integrated with buildings, a balanced relationship between requirements and design needs to be considered, and traditional experimental research methods are unable to consider several objectives simultaneously and achieve design optimization. Parametric design and multiobjective optimization methods can achieve energy and environmental objectives for several building solutions, perform comparative analysis, and optimize the design to predict the best solution [22–26].

Solar-concentrating photovoltaic modules have the advantages of high efficiency and improved indoor light environment. After integration with the building, it is possible to meet the energy output while achieving a balanced design of multiple demand goals, such as indoor light environment and energy efficiency, by changing various parameters, such as the size of the concentrating modules, the form of integration with the building, and

the regulation method, which not only meets the requirements of developing low-carbon sustainable buildings but also creates a comfortable office environment and beautiful building for workers.

In this study, based on the preliminary design of the integration of the solar-concentrating skin and the building, we use parametric and multiobjective optimization methods to construct and test the performance and design the scheme of the space composed of the solar-concentrating skin. The following issues are explored:

1. The equilibrium relationship between the indoor light environment and the energy output of the solar-concentrating skin under different states of dynamic concentrating skin, trying to solve the optimal integration problem of dynamic concentrating skin and building integration, providing different design solutions for integration and reducing energy consumption and carbon emissions.
2. The intrinsic connection between the design parameters and the performance optimization target determines how the design parameters affect the performance optimization target, optimization range, and weight size of the design parameters by analyzing the relationship between the parameters and the performance.
3. Through the optimal design of a dynamic concentrating epidermis, we attempt to construct a multiobjective optimization technology framework applicable to dynamic skin using the design–simulation–analysis method to solve the single-threaded optimization design.

2. Methodology

2.1. Optimize Platforms and Processes

This section explains the design decision process for the optimization and the required optimization platform. This research relies on the Ladybug toolkit under the Rhino Grasshopper parametric modeling platform and the Octopus multiobjective optimization platform to optimize the design of multiple objectives. The Ladybug toolkit already has a built-in kernel of existing and proven simulation tools [27,28]. Octopus is a multiobjective solution platform that is stable, interactive, and efficiently visualized; it combines the Pareto optimal principle and genetic algorithms to generate a custom number search for solution generation, offering a wide range of possibilities for designers to choose from for multiobjective problems [29]. The Octopus platform can be used to search for optimal design solutions by controlling multiple metrics and is suitable for multiobjective studies on the indoor light environment and energy efficiency of the solar dynamic concentrating skins [30–35].

The solar dynamic concentrating skin multiobjective optimization process and the required tools are shown in Figure 1, including three stages. The first stage was the construction of the solar dynamic concentrating skin, including the design of the solar-concentrating module, the design of the solar dynamic concentrating skin, and the construction of the parametric information model in three parts. The design of the solar-concentrating module and solar-concentrating skin was determined based on integration with the building. The purpose of the construction of the parametric information model is to determine the design parameters and assign them to the study object. The design parameters determine the performance size when the performance simulation is performed. The second stage is the mapping of environmental information to model information and the establishment of optimization functions for the simulation of the light environment and capacity efficiency. This includes the determination of the evaluation objective function, calculation of the light transmission equivalence of the solar-concentrating module, and assignment of weather files and materials. The purpose of determining the evaluation function is to quantitatively and objectively evaluate the variability of the optimized performance. Weather files and material properties significantly influence the distribution of light. The transmittance calculation of the solar-concentrating module is primarily used to solve the construction problem of the Fresnel material. The third stage uses data analysis software to study the influence of design parameters on performance, and finally provides different optimization solutions.

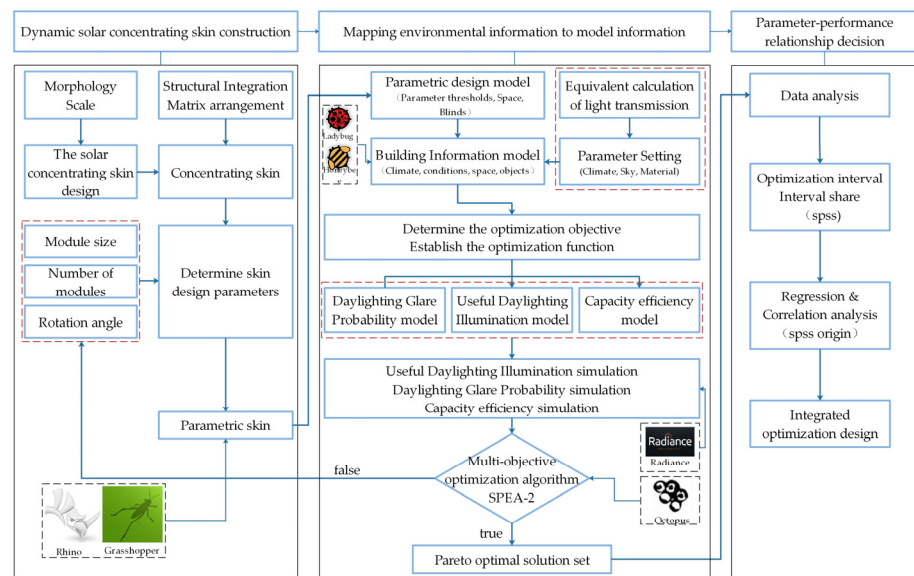


Figure 1. Research workflow.

2.2. System Description

2.2.1. Design of BICPV

The linear transmittance solar-concentrating module designed in this study is based on the theory of Fresnel concentrating, which concentrates direct light and transmits scattered light. Considering the scale, form, and characteristics of the selected light concentrating technology, combined with the parts integrated with the building, through repeated modifications and optimization of the solar-concentrating module, the final design of the solar-concentrating module for a general building window composition is shown in Figure 2.

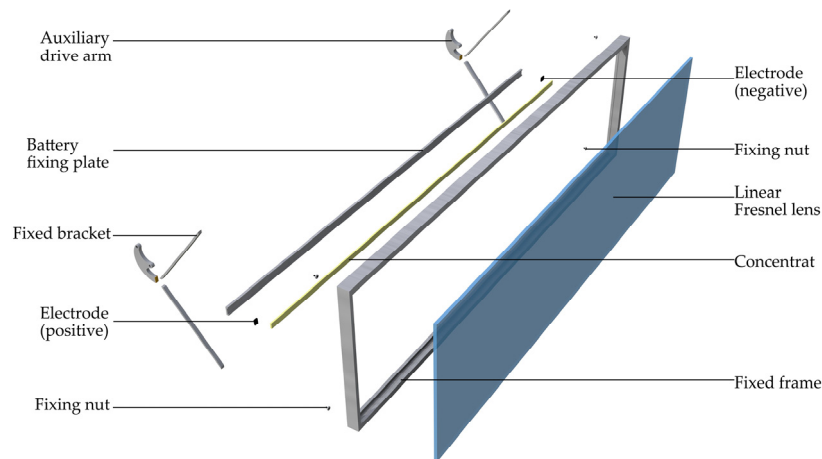


Figure 2. Design of the to-be-integrated concentrating module.

The designed solar-concentrating modules are arranged in an orderly manner, integrated with the building, and made to track the position of the sun in the working state by sensors to form a solar dynamic concentrating skin. To ensure the stability and durability of the solar-concentrating skin, the solar dynamic concentrating skin was placed between the double glazing, as shown in Figure 3.

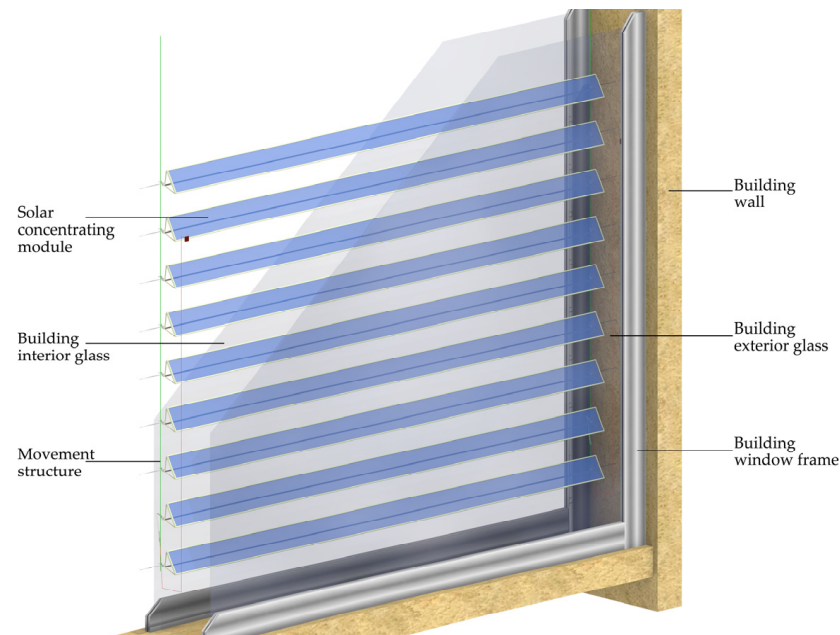


Figure 3. Dynamic concentrating skin integration system.

To study the effect of the change process of the solar dynamic concentrating skin on indoor light environment and energy efficiency, the standard office space in Xuzhou City, Jiangsu Province (lat: 34.28, lon: 117.15) was selected as the simulation object of light environment and energy efficiency in this study. This office space has a single, south-facing, plain, and fixed window with integrated solar dynamic concentrating skin at the window. The solar-concentrating skin is located between the double glazing; the thickness of the double glazing is 6.0 mm and the spacing is 300 mm. The depth of the office space is 6.0 m, the opening is 3.3 m, and the net height is 3.6 m. The building window faces south, the window height is 3.0 m, the window width is 3.0 m, and the distances between the edge of the window and the upper, lower, left, and right sides of the south-facing wall are 0.20 m, 0.40 m, 0.15 m, and 0.15 m, respectively. An office space with integrated solar-concentrating skin is illustrated in Figure 4.

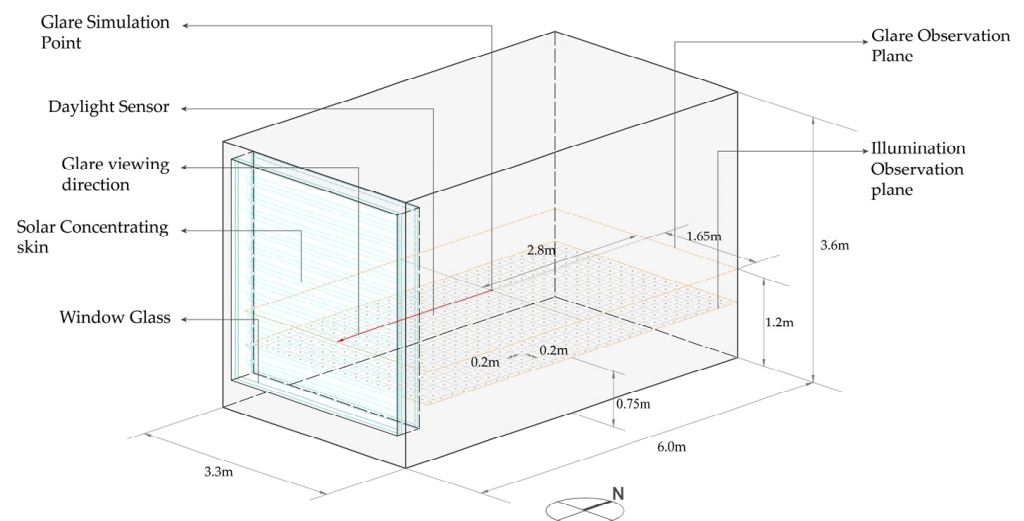


Figure 4. Office space with integrated solar-concentrating skin.

2.2.2. Constructing Parametric Information Models

(1) Determining design parameters

Compared with office spaces with or without shading measures, the shading form, location, and size of the area have a direct impact on the indoor light environment. In this study, the solar-concentrating skin built between the double glazing exhibited shading and concentrating effects on the indoor light environment, similar to a shading element. Therefore, the size of the solar-concentrating module, size of the solar-concentrating skin composed of multiple solar-concentrating modules, and rotation angle of the solar-concentrating skin in the process of tracking the sun will change the distribution of light and affect the creation of an indoor light environment in an office space. The size, number, and angle of the solar-concentrating modules also affected the capacity efficiency of the solar-concentrating skin without considering the self-shading case. In summary, three factors, namely the size of the solar-concentrating module, number of arrays of the solar-concentrating module, and rotation angle of the solar-concentrating module, were considered as the design parameters for multiobjective optimization in this study.

(2) Constructing parametric models

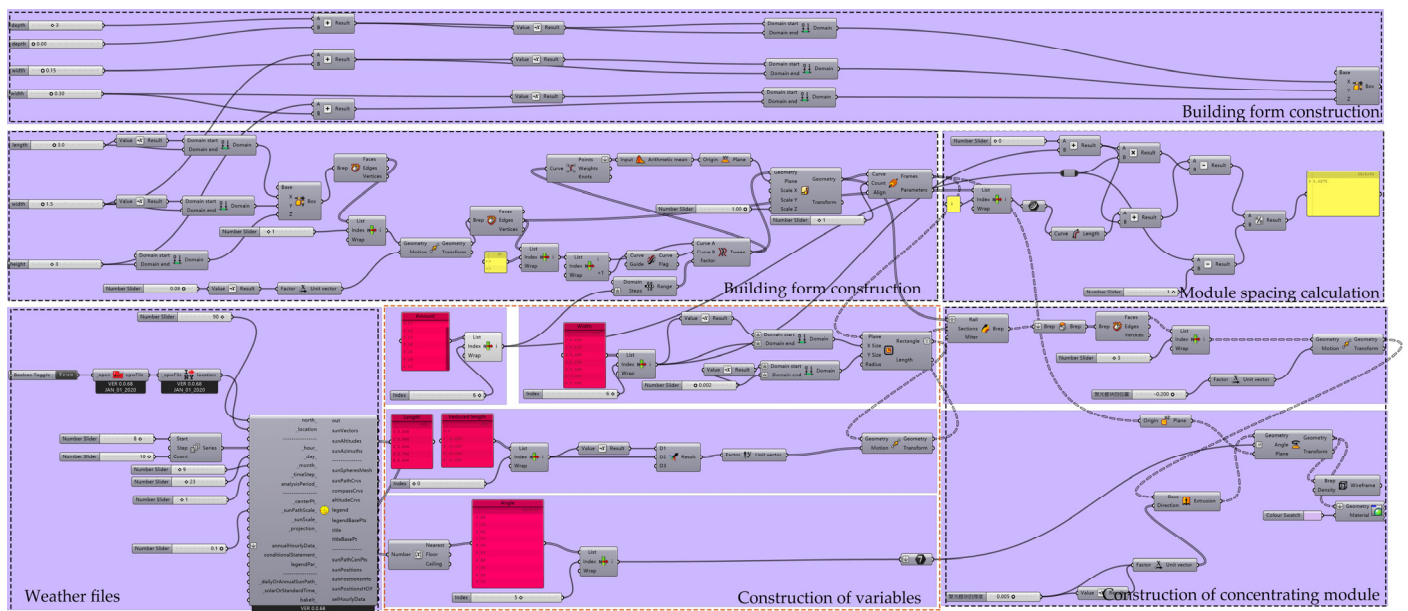
To consider computer performance, a parametric model of the motion and support structure that has no effect on the software simulation, the solar sensor that can be achieved through software settings, and the solar-concentrating cell that can be achieved by indirect calculation is simplified for modeling, and double glazing—which has a large impact on light—can be parametrically constructed. The linear Fresnel lens solar-concentrating module, which has a direct impact on the concentration and scattering of light, needs to be equated for its modeling and will be highlighted below.

First, the office space was parametrically modeled, and the length, width, and height were input to obtain the office space shape. Then the “list item” operator in Grasshopper was used to extract the south-facing wall of the building, and the four sides of the south-facing wall were offset 0.20 m, 0.40 m, 0.15 m, and 0.15 m, respectively, from the upper, lower, left, and right side of the wall as the protective structure of the window, and the middle part was used as the scope of the solar-concentrating skin. The “list item” operator was used to extract the top and bottom edges of the south-facing face of the original form, and its spacing was used as the maximum capacity spacing of the concentrating module. The “tween curve” operator was used to equidistantly separate the top and bottom lines according to the width of the spotting module to obtain the location of the plane where the spotting module is located. Then, the “rectangle” operator was used to draw the cross-section of the solar-concentrating module in the vertical plane of the split line, and “sweep 1” operator was used to draw the solar-concentrating module according to the length parameter. The centerline of the length of the solar-concentrating module is extracted as the rotation axis of the solar-concentrating module to track the rotation of the sun position.

The ratio of the maximum spacing to the width of the solar-concentrating module was used as the number parameter in the design (number of equally spaced dividers). The lengths of the two lines above and below are used as the length parameters of the solar-concentrating module, and the width parameter is closely related to the number parameter. The maximum number of solar-concentrating modules is 17. The distance between the two modules is 2.75 mm, the width is 160 mm, and the length is 3000 mm. Considering the large number of orthogonal matrices and subdivisions of design parameters that affect the calculation time, all design parameters were explored in their decreasing form in this study. The number of solar-concentrating modules was chosen to be decreasing in a single quantity, while the width and length of window modules were chosen to be decreasing by 10 mm and 100 mm, respectively. The angle was rotated to simulate the weather and climate file of the area where the object was located and selected according to the actual simulation time period and sun position. The specific settings of the design parameters are listed in Table 1, and the model was constructed, as shown in Figure 5.

Table 1. Setting of each design parameter of the spotlight module.

Solar-Concentrating Module Design Parameters	Calculation Range	Parametric Design Basis	Corresponding Slide Bar Parameters
Size of the solar-concentrating module	Reduced length of the solar-concentrating module (m) 0.4 (2.6), 0.3 (2.7), 0.2 (2.8), 0.1 (2.9), 0(3)	The calculation range is determined by the maximum length of the window length	4, 3, 2, 1, 0
Quantity of solar-concentrating modules (number)	Reduced width of the solar-concentrating module (m) 0.1, 0.11, 0.12, 0.13, 0.14, 0.15, 0.16	The calculation range is determined by the maximum width of the module when the window height accommodates the maximum number of modules	0, 1, 2, 3, 4, 5, 6
Rotation angle of the solar-concentrating module (°)	11, 12, 13, 14, 15, 16, 17	The calculation range is determined by the maximum amount calculated from the window height	0, 1, 2, 3, 4, 5, 6
	24, 35, 45, 53, 56, 53, 46, 36, 25, 13	The calculation range is determined by the calculation time period and the direction of solar radiation	0, 1, 2, 3, 4, 5, 6, 7, 8, 9

**Figure 5.** Parametric model construction procedure and design parameters.

2.3. Constructing Evaluation Functions

2.3.1. Determine Optimization Objectives

Before proceeding with the energy model construction, the performance optimization objectives under the design parameters must be determined to purposefully transform the base model into a performance model. The most important feature of solar-concentrated skins over ordinary skins is that they can generate energy and change the light in the room while shading for indoor light environment problems, such as glare near the window, insufficient illumination deep in the room, and insufficient natural light in the effective range during working hours. Combining regulatory standards, light environment evaluation metrics, and metrics suitable for evaluating dynamic skin lighting performance [36–39], daylight glare probability (DGP) and useful daylight illuminance (UDI) are selected as the indoor light environment optimization objectives. The capacity efficiency of the solar-concentrating skin was used as the third optimization objective. The optimization target selection and criteria are listed in Table 2.

Table 2. Performance optimization target selection and criteria.

Optimization Goals	Definition Description	Suitable Range	Evaluation Criteria
Daylight glare probability (DGP)	Refers to the glare indicator used to describe the probability of uncomfortable glare in the room, and is based on DGI, CGI indicator updated (2006) [38]	DGP < 0.35	DGP < 0.35: imperceptible glare; 0.35 ≤ DGP < 0.40: perceptible glare; 0.40 ≤ DGP < 0.45: disturbing glare; DGP ≥ 0.45: unbearable glare [40]
Useful daylight illuminance (UDI)	Refers to the range of illumination values that can meet the normal visual work of workers	500 lux–2000 lux	Effective lighting illumination value 100 lux–2000 lux [39]
Capacity efficiency (CE)	Refers to the energy value generated by the concentrating epidermis after absorbing direct light	—	The greater the energy efficiency, the better

2.3.2. Construction of Optimal Objective Evaluation Function

In order to investigate the relationship between the design parameters of the solar-concentrating skin and the multiobjective optimization, the results during the time period of the entire year were selected as the evaluation indices in the study, and the simulation procedures for the evaluation of each optimization objective are shown in Figure 6. Among the selected indoor light environment optimization targets, UDI belongs to the dynamic evaluation index of natural lighting throughout the year, whereas DGP is a static index at a certain moment. To evaluate the light environment optimization targets at the same level, improve the computer's calculation speed of the DGP, and achieve the optimization purpose of reducing glare instead of eliminating it, this study simplifies the calculation of the DGP index. In clear sky, the glare value is maximum at 12:00 noon every day, and if the glare is reduced with a large probability at 12:00 noon, it can represent the achievement of the optimization purpose. First, we calculated the glare magnitude at 12 noon every day of the year under unobstructed conditions, and then selected the moments with large values of glare concentration in different seasons of the year for calculation and simulation and took the ratio of the number of days less than 0.4 in the DGP simulation results to the total number of days simulated as the optimization target. The viewpoint looking out of the window at a 1.2 m elevation from the center point of the indoor floor was selected as the simulation point. The glare evaluation function is given by Equation (1).

$$f_1(a) = \frac{\sum_{i_x}^{n_x} DGP_{<0.4_{i_x}}}{n_x} \times 100\% \quad (1)$$

where $f_1(a)$ stands for glare target evaluation function (%) and n_x is the number of calculations at 1.2 m elevation of the center point of the indoor floor at the time of selection. $DGP_{<0.4_{i_x}}$ is the i -th DGP simulation result less than 0.4 in the selected time.

UDI was selected at 0.75 m elevation from the floor of the office space as the grid analysis surface for natural lighting performance, with a grid size of 0.2 m, and the timeshare of the illuminance value satisfying in the simulation results as the optimization target. The UDI evaluation function is given in Equation (2).

$$f_2(b) = \frac{\sum_i^n UDI_{100-2000_i}}{n} \quad (2)$$

where $f_2(b)$ is the UDI target evaluation function (%) and n represents the number of illuminance calculation points on the horizontal working surface at 0.75 m elevation indoors. $UDI_{100-2000_i}$ is the percentage of time that the i -th calculation point satisfies the 100 lux–2000 lux condition.

An equivalent conversion method was used in this study to optimize the solar-concentrating skin capacity efficiency. The solar-concentrating skin has the property of concentrating and absorbing direct light and transmitting scattered light, while it can gen-

erate energy by absorbing direct light for concentrating. Thus, the energy efficiency of the solar-concentrating skin can be equivalent to the amount of concentrated direct light. The sunlight propagates in the form of electromagnetic radiation, and the solar-concentrating characteristics also use radiation for energy production. The direct solar radiation flux can be used to achieve an equivalent conversion to concentrating energy production. The calculation of direct solar radiation flux is based on a special meteorological dataset for the thermal environment analysis of Chinese buildings and the radiation flux obtained by importing EPW files with Ladybug tools. Direct solar radiation fluxes were obtained by analyzing and filtering the sunless hours at night for each hour of the day from 8:00 a.m. to 5:00 p.m. throughout the year. Because the solar-concentrating skin cannot convert all the radiation flux into energy, the annual direct radiation flux is accumulated and multiplied by the area of the solar-concentrating skin and the solar-concentrating efficiency [7] to obtain the annual capacity efficiency of the solar-concentrating skin. The evaluation function of the capacity efficiency of the solar-concentrating skin is shown in Equation (3).

$$f_3(c) = \sum_t^T \left[\sum_i^n I_{DH_i} \right] \times S \times \eta \tag{3}$$

where $f_3(c)$ is the evaluation function of the capacity efficiency of the solar-concentrating skin (w/h), I_{DH_i} is the direct radiation flux at time i on day t of the year, n is the calculation period, and T is the number of days in the year. S is the area of the solar-concentrating skin, and η is the solar-concentrating efficiency of the solar-concentrating skin.

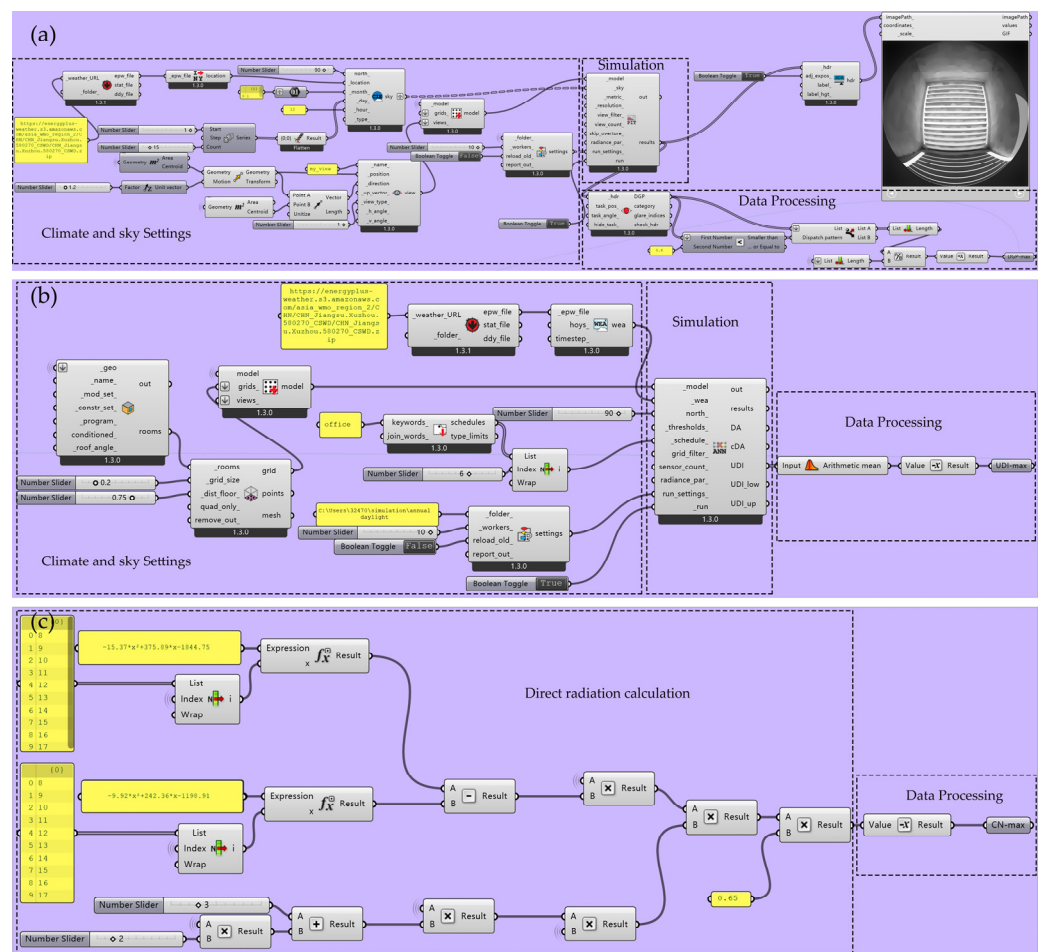


Figure 6. (a) Daylight glare probability target calculation procedure. (b) Useful daylight illuminance target calculation procedure. (c) Annual capacity efficiency target calculation procedure.

2.4. Simulation Parameters Setting

2.4.1. Climate Data and Sky Models

The selection of climate data affects the accuracy of the indoor lighting environment simulations. The free EnergyPlus Weather Data (EPW) file provided by the U.S. Department of Energy's EnergyPlus website is used more frequently at home and abroad [41], and the weather data file provided by this website can provide accurate climate analysis for academic institutions and laboratories. In this study, the EPW meteorological file of Xuzhou City, Jiangsu Province, was obtained through this website to ensure that the area to which the simulated space belonged was highly similar to the climatic conditions of the real building space. For the sky model, the internationally used CIE standard sky was selected, and sun-type sunny sky was used as the real sky model for the simulation.

2.4.2. Calculation of the Equivalent Model of the Concentrated Light Surface

The solar-concentrating module is a linear Fresnel lens with internal grooves, which cannot be accurately constructed for the grooves during the simulation and affects the given material; therefore, it needs to be equated. The solar-concentrating skin converges direct light for energy production, reducing the amount of direct light entering the room. Therefore, the linear Fresnel lens can be equated to a low-transmittance ordinary glass material where only scattered light can enter the room. Under ideal conditions, only the ratio of the scattered luminous flux through ordinary glass to the total luminous flux needs to be calculated. The transmittance was calculated as the scattered light flux in the full wavelength band and not the scattered light flux in the visible wavelength band. Given that the full-band luminous flux in the simulated environment cannot be obtained in real time, and the time-by-time radiant flux provided by the EPW file is the full-band solar radiation, the solar radiant flux can represent the luminous flux for simplified calculation of the glass transmittance. The focus of this study is on the optimal design and technical framework construction of solar-concentrating skin; therefore, this study will calculate the transmittance of low-transmittance ordinary glass using the scattered radiation flux obtained from the EPW file.

The sun position and climate conditions determine the magnitude of the scattered luminous flux, and the sun position must be tracked during the simulation period to calculate the scattered luminous flux at the simulation moment. Therefore, based on the rotation angle of the solar-concentrating skin obtained from the EPW file during the simulated period in the above design parameters, the scattered luminous flux projected onto the solar-concentrating skin was calculated to achieve the equivalence of the optical properties of the solar-concentrating module composed of a linear Fresnel lens. The detailed calculation is given in Equation (4).

$$\tau = \frac{I_{dh}}{I_{Th}} \times 100\% \quad (4)$$

where τ is the light transmission rate of ordinary glass material, I_{dh} is the scattered radiation flux, and I_{Th} is the total radiation flux.

2.4.3. Material Parameters and Optimization Platform Setting

Performance simulations using Ladybug and Honeybee require that the parametric model be given radiance material and converted to a recognizable Honeybee model. The types of materials included office space walls, double glazing, and solar-concentrating skins. The walls and double glazing used preset materials from the simulation library, and the solar-concentrating skins used ordinary glass materials with different scattered luminous flux ratios after equivalent modeling. The parameter settings for each material are presented in Table 3.

Table 3. Each material parameter setting.

Material Assignment Type	Parameter Setting
Wall	0.5, 0.5, 0.5, 0, 0
Double glazing	0.872, 0.872, 0.872, 0, 0
The solar-concentrating skin	0.450, 0.450, 0.450, 0, 0, 0, 0.300 (“ τ ” calculated by Equation (4))

In this study, using the Octopus multiobjective optimization platform, a genetic algorithm was used to search for the Pareto optimal solution set satisfying the performance metrics and design parameter equilibrium. The O-side of the Octopus module operator is the performance optimization target port, and the G-side is the parameter variable gene port. The three covariates of solar-concentrating skin—size (length and width), amount, and angle—were connected to the O-port. Because the Octopus operator is optimized only in the direction of the minimum value, the three metrics of DGP, UDI, and solar-concentrating skin capacity efficiency are connected to the G-terminus by algebraic operations. Based on the combination of optimization objectives, simulation accuracy, and calculation time, specific parameters are entered in the Octopus module operator panel (see Table 4.), and then the optimization calculation begins.

Table 4. Technical data of Octopus module operator.

Calculation Module	Parameter Name	Input Parameter Setting
	Genome	Corresponding slide bar parameters (Table 1)
	Octopus	Daylight glare probability (DGP) Useful daylight illuminance (UDI) Capacity efficiency (CE)
Octopus	Population size	100
	Max generation	0
	Elitism	0.500
	Mut.Probability	0.200
	CrossOver Rate	0.800

3. Results

3.1. Optimization Interval Analysis

The experimental simulation was run for 196 h with 50 iterations of computation, 191 solution sets were obtained for the gene pool, and the optimization results gradually converged to a convergence trend after the 15 th generation. The multiaxis view in Figure 7 shows that each performance index value gradually concentrates from the maximum value to the minimum value, and the optimal solution set floats and gradually concentrates near the minimum value. The simulation results show that the DGP calculation range is 0.00–1.00; the UDI rounding calculation range is 42.45–61.80%; and the capacity efficiency rounding calculation range is 13.01 Kw·h–332.39 Kw·h.

Because the ratio of the number of days less than 0.4 in the DGP simulation results in the total number of days simulated was used as the optimization target, including the number of days that reduce glare but do not meet the requirement, the percentage of the optimization target was 0. Therefore, 32 sets of Pareto optimal solutions in the 15th-generation convergence state were selected, and the 32 sets of solutions were ranked with the unfavorable factor index in the light environment index as the main optimization objective. The group with a DGP percentage of 0 was excluded to obtain 26 sets of Pareto optimal solutions (see Table 5). The optimal distributions of the 26 sets of optimized solutions are shown in Figure 8. The design parameters and performance objectives of the optimal solution were statistically analyzed to obtain the optimal interval and maximum percentage of parameters, as shown in Table 6.

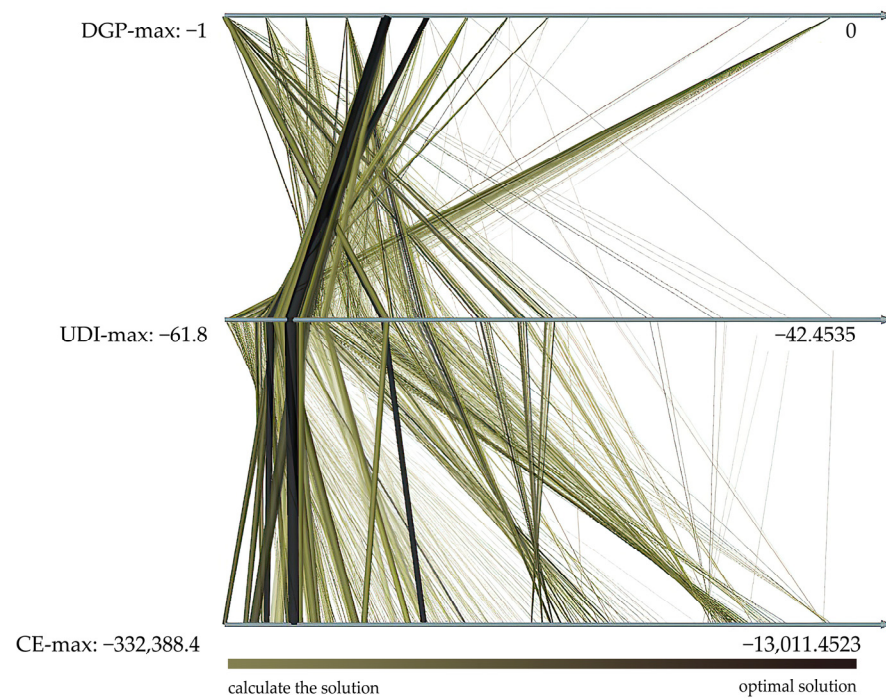


Figure 7. Optimized trend multi-axis view.

Table 5. 26 sets of optimized solution cases.

Number	Amount (Number)	Width (m)	Length (m)	Angle (°)	DGP (%)	UDI (%)	CE (Kw·h)
1	16	0.14	2.6	24	100	58.37	42.05
2	15	0.14	2.8	25	87	58.78	59.11
3	15	0.14	3	25	87	58.60	63.33
4	15	0.15	3	25	93	57.57	67.85
5	15	0.15	2.9	25	87	57.70	65.59
6	16	0.13	3	25	93	58.77	62.73
7	16	0.14	2.8	25	93	57.84	63.05
8	16	0.15	2.6	25	100	57.32	62.73
9	16	0.13	2.7	25	87	59.16	56.45
10	16	0.15	2.7	25	100	56.77	65.14
11	16	0.13	2.8	25	93	58.96	58.54
12	17	0.13	2.9	25	87	57.71	64.42
13	17	0.13	3	25	87	57.59	66.65
14	17	0.15	2.6	36	80	57.89	139.5
15	17	0.14	2.6	36	80	58.96	130.2
16	17	0.16	2.9	45	100	56.75	227.87
17	17	0.16	3	46	100	56.65	259.35
18	17	0.16	2.7	53	73	59.97	285.37
19	17	0.16	2.8	53	73	59.73	295.94
20	17	0.16	3	53	73	59.32	317.08
21	17	0.16	2.6	53	73	60.16	263.54
22	16	0.16	3	56	53	60.82	312.84
23	17	0.16	2.7	56	67	60.52	299.15
24	17	0.16	2.8	56	67	60.35	310.23
25	17	0.16	3	56	67	60.14	332.39
26	17	0.16	2.9	56	67	60.25	321.31

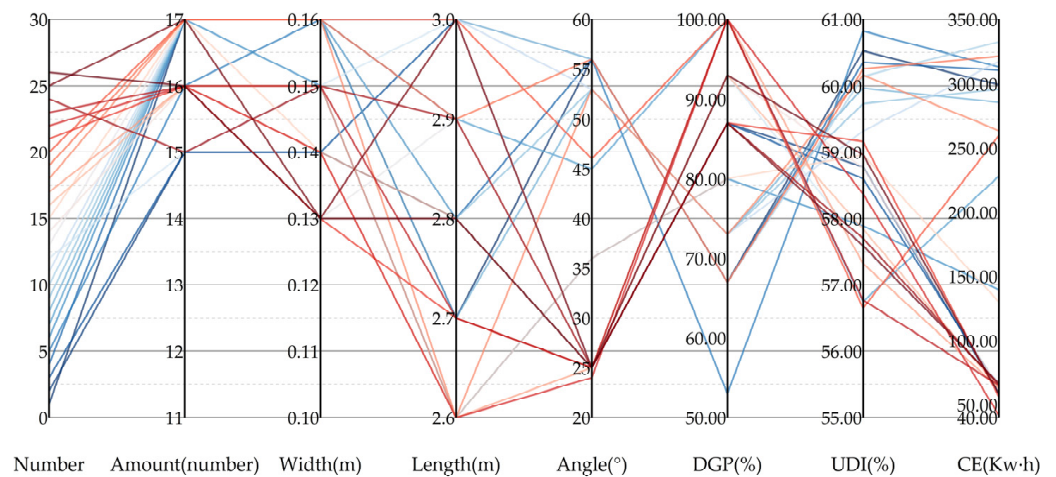


Figure 8. Optimal distribution of 26 sets of optimal solutions.

Table 6. Design parameters and performance target optimal intervals and percentages.

Name	Parameters and Performance Indicators	Optimal Interval	Percentage of Maximum Parameters (Interval) and Percentage	Percentage of Minimum Parameters (Interval) and Percentage
Design parameters	Length of the solar-concentrating module (m)	2.6–3.0	3.0, 31%	2.7, 15%
	Width of the solar-concentrating module (m)	0.13–0.16	0.16, 42%	0.13, 19%
	Quantity of solar-concentrating modules (number)	15–17	17, 54%	15, 15%
	Rotation angle (°)	24–56	25, 46%	56, 4%
Performance indicators	DGP (%)	53–100	80–90, 31%	50–60, 4%
	UDI (%)	56.65–60.82	56–60, 77%	60–60.82, 23%
	CE (Kw·h)	42.05–332.39	42.05–90, 50%	100–332.39, 50%

As shown in Table 6, the maximum percentage of DGP ranges from 80% to 90%, the maximum percentage of UDI ranges from 56% to 60%, and the maximum percentage of concentrating efficiency ranges from 42.05 Kw·h to 90.00 Kw·h. Among the design parameters, the maximum percentages of the size and number of solar-concentrating module parameters were in the lower part of the analysis range, and the rotation angle parameters were in the upper part of the analysis range. The results show that the larger the number of solar-concentrating modules and the smaller the number of rotation angles, the more favorable the performance optimization objective; thus, when the parameters of the module are in the range of Table 6, it is the best parameter for the module and the design of integration with the building. For example, the module size in 3 m × 0.14 m and the integration angle in 25° is the best design parameter for the module, which can obtain a better indoor light environment at the same time of obtaining the maximum energy. The actual design is usually chosen for different purposes, all of which should be based on the simulated optimal parameters to choose the design parameters that are most beneficial to building performance. When the purpose is based on maximizing energy output, a larger angle or larger width should be chosen within the simulated optimal parameters to obtain the maximum energy output. However, the optimal parameters of the simulation are obtained based on the weather climate of the simulated location and are not applicable to the integrated design of other locations, so further solving is required when changing locations.

3.2. Correlation Analysis of Performance Indicators and Design Parameters

To investigate the relationship between each optimization objective and other performance objectives and design parameters when optimal, first, 26 sets of data for the three performance indicators were analyzed by regression fitting, and the optimized relationship of the three performance indicators was obtained, as shown in Figure 9. From this relationship, it is concluded that the overall trend of DGP optimization is between 50% and 80%, UDI and CE both have higher performance and gradually show a decreasing trend, and UDI and CE decrease as DGP increases. The set of optimized solutions in this interval is also smaller, although it is in the optimal solution, which may be mainly because the optimization prefers the optimal solution for a certain indicator. When the DGP is between 80% and 100%, the UDI tends to rise and then decrease as the DGP increases, and the CE tends to fall to the lowest point and then increase as the DGP increases. Analysis of the dependent variable may be the main reason that the angle of rotation of the spotlight skin decreases, and the surface area of the skin increases, resulting in a large amount of light being absorbed by the solar-concentrating skin of light indoor effective illumination is reduced, and the energy produced increases. From the set of 26 optimal solutions, the typical solutions with three optimization objectives, each optimal and one integrated optimal, were selected, and their positions on the regression curves were analyzed, as shown in Figure 9. The case parameter indicators are shown in Table 7. In the UDI optimal solution, DGP is the smallest and CE is also higher; in the DGP optimal solution, CE is the smallest and UDI is above 58%; in the CE optimal solution, both DGP and UDI are above 60%; in the combined optimal solution, each index has a high value and CE and UDI intersect at the regression curve.

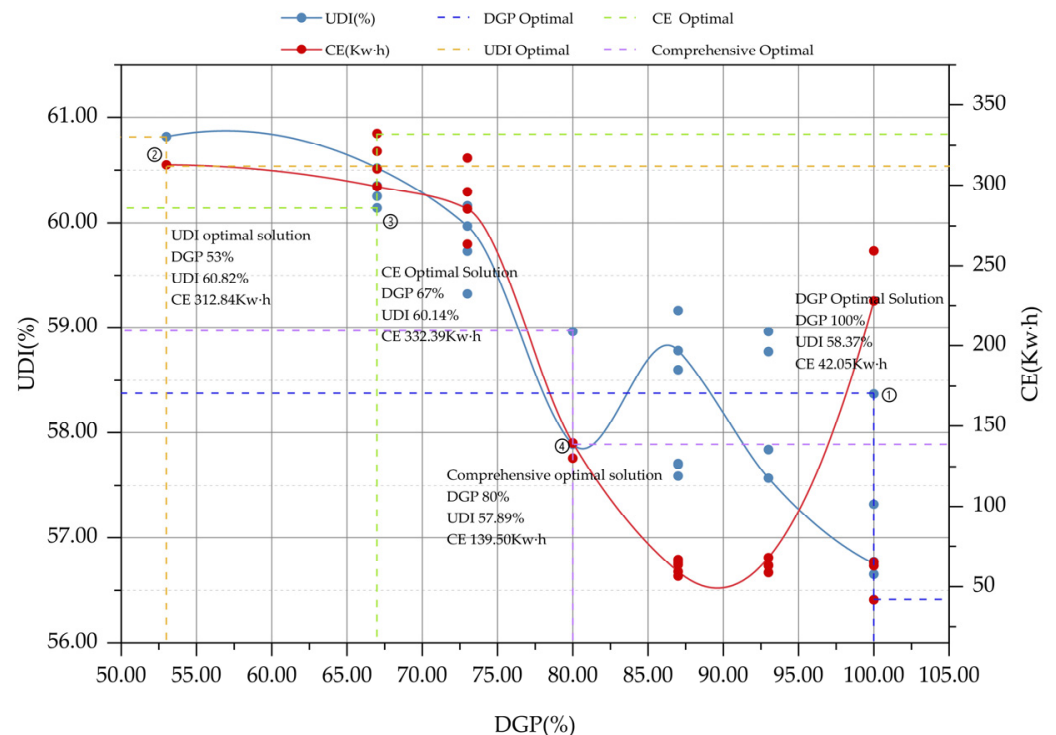
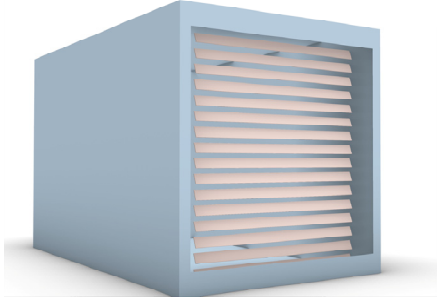
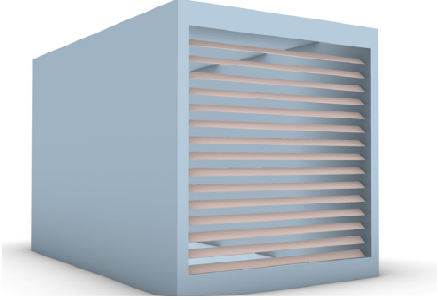
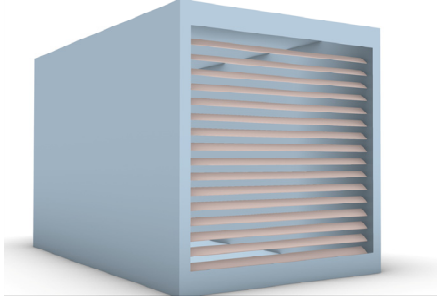
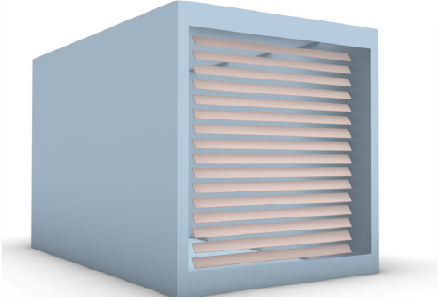


Figure 9. Performance metrics regression analysis.

Table 7. Optimization case parameter indicators.

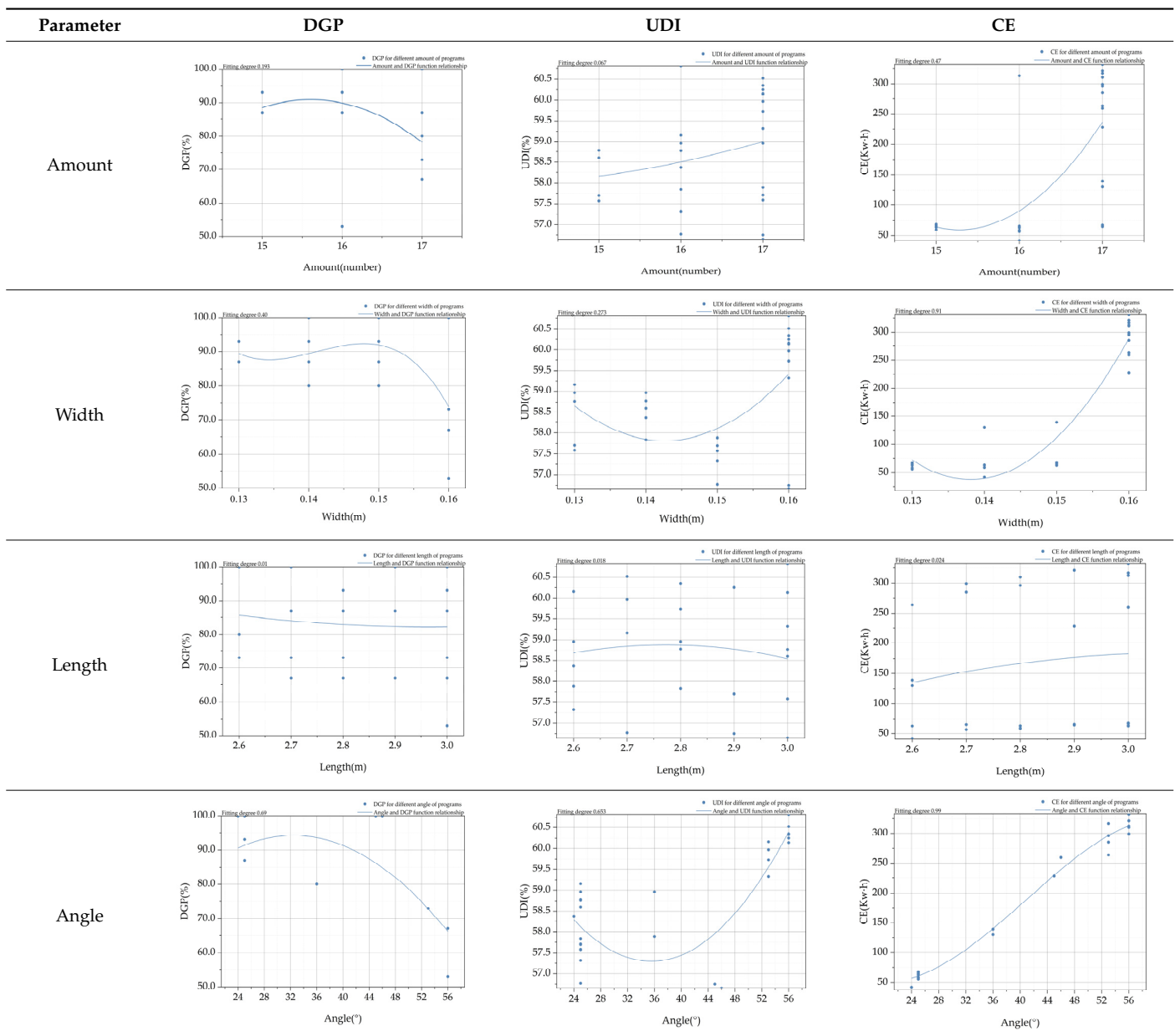
1-DGP Optimal Solution				2-UDI Optimal Solution			
DGP _{<0.4}	100%	Module size	2.6 m × 0.14 m	DGP _{<0.4}	53%	Module size	3.0 m × 0.16 m
UDI _{100–2000LUX}	58.37%	Module amount	16	UDI _{100–2000LUX}	60.82%	Module amount	16
CE	42.05 Kw·h	Rotation angle	24°	CE	312.84 Kw·h	Rotation angle	56°
							
3-CE Optimal Solution				4-Comprehensive optimal solution			
DGP _{<0.4}	67%	Module size	3.0 m × 0.16 m	DGP _{<0.4}	80%	Module size	2.6 m × 0.14 m
UDI _{100–2000LUX}	60.14%	Module amount	17	UDI _{100–2000LUX}	57.89%	Module amount	17
CE	332.39 Kw·h	Rotation angle	56°	CE	139.50 Kw·h	Rotation angle	36°
							

The correlation analysis between each variable and each performance index (Figure 10) showed that the correlation coefficient between DGP and UDI was 0.883, a high negative correlation; the correlation coefficient between DGP and capacity efficiency was 0.750, a high negative correlation; and the correlation coefficient between UDI and capacity efficiency was 0.629, a moderate positive correlation. The main reason is that the DGP and UDI are calculated from scattered light and the capacity efficiency is calculated from direct light when the solar-concentrating skin is performing capacity and light harvesting. The negative correlation between UDI and DGP may be because when the DGP is larger, there is less glare in the room, which weakens the light and leads to insufficient effective illumination. Among the covariates, the angle covariate had a high correlation with the three performance indicators of DGP (-0.755), UDI (0.668), and capacity efficiency (0.994); the width covariate had a moderate correlation with DGP (0.500) and a high correlation with capacity efficiency (0.848); the number covariate had a high correlation with capacity efficiency (0.648), and the length covariate had a high correlation with performance metrics but no correlation. The regression analysis of each covariate with the performance indices yielded a functional relationship between the indices and performance, as shown in Table 8. From the fit of the curves, it can be concluded that the number and length variables have no obvious relationship with each performance index, and the angle and width variables have a more obvious relationship with each performance index. The distribution of the 26 solution sets (Figure 8) and the regression curves show that among the angular variables, the solution sets are mainly located at the two ends of the curve, 24° – 26° and 52° – 56° , respectively, and the latter has higher values on the curve than the former. The main reason is probably that when the angle is small, the concentrating module blocks less direct light, and more daylight enters the room so that the UDI of the room to meet the work is low, and the DGP near the window has a small value and a high optimization rate. The angle

is larger at noon, the concentrating module shades more direct light, the light entering the room becomes less, the UDI of the room to meet the work is increased, the value of DGP is small, and the optimization rate becomes smaller. The width variables are more uniformly distributed on the curve, and the variables with more distribution in the UDI and CE indicators are 0.16 m and the values of UDI and CE at 0.16 m are higher than other width variables. The main reason for this is that when at 0.16 m, there is the more blockage of direct light, so the values of UDI and CE become bigger. The value of DGP is the small, and the DGP optimization rate is smaller.

Since the performance targets are influenced and constrained by multiple variables, combining the fit of the regression function, the magnitude of the correlation between each parameter and the performance index, and the magnitude of the trend of the fitted curve, it is concluded that the angle parameter is the main consideration in the multiobjective design of the concentrating skin, followed by the width parameters, whose amount and length can be disregarded under small variations.

Table 8. Parameter–performance relationship.



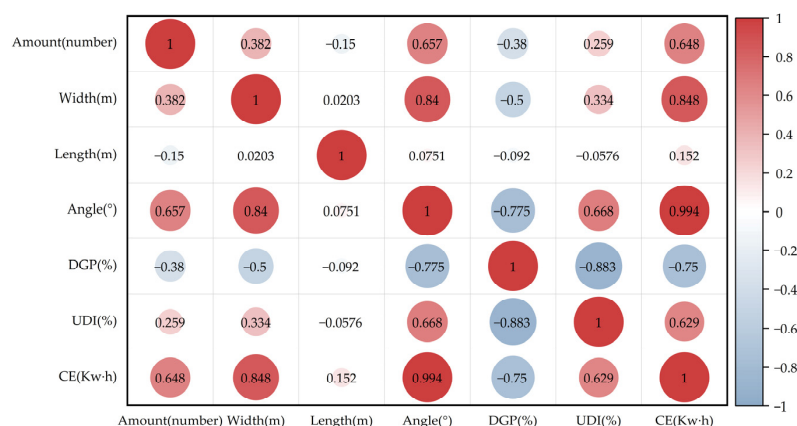


Figure 10. Correlation between each variable and each performance indicator.

3.3. Comparative Analysis of Integrated Solar-Concentrating Skin, Integrated Common Skin, and No Integrated Skin

The DGP, as an important indicator of unfavorable factors in an indoor light environment, is considered the main optimization target. Therefore, the 26 sets of solution sets are divided into three parts according to the magnitude of DGP values, and then the solar-concentrating skin scheme with higher optimization rate and other variables that are also better is selected from the three parts for a comparative study with the skin without integration and the skin with common sunshade module integration. From the data in Table 9, it can be seen that among the three scenarios, the scenarios with no skin and ordinary skin cannot produce energy because they cannot converge and absorb the sun-rays, whereas solar-concentrating skin has a more efficient energy output, and the annual capacity efficiency can be as high as 332.39 Kw·h. In the DGP target simulation time period, the percentage of no skin scheme appearing less than 0.4 is 0, indicating that both will show glare. In the normal skin scheme and the solar-concentrating skin scheme, the percentage of DGP of the normal skin scheme is still 0, whereas the reduction rate of glare by the concentrating skin reaches approximately 70% on average. The main reason may be that ordinary skins do not reduce direct light but change the distribution of direct light through reflection of the material, resulting in glare, whereas solar-concentrating skins absorb direct light through their own characteristics, reducing the probability of glare. For the UDI, the skinless solution has a lot of light entering the room; however, it is not a sufficiently effective illumination to satisfy the indoor workers’ work. The solar-concentrating skin and ordinary skin solutions significantly increase the effective illumination of the room by absorbing direct light and blocking part of the unfavorable light, improving illumination in the range of approximately 10%. The difference between normal skin and concentrating skin in terms of UDI is small; however, normal skin has a significant impact on the blockage of the field of view compared to concentrating skin, which has a better performance ability. To more clearly demonstrate the three skin scenarios under different covariates, Scheme 2 was selected for visualization and comparison, as shown in Table 10.

Table 9. Comparison data of different solutions.

Scheme Name	Performance Goals	Solar-concentrating Module	General Module	No Module	Relative Optimization Value 1	Relative Optimization Value 2
Scheme 1	DGP (%)	53	0	0	53	53
	UDI (%)	60.82	60.72	50.92	0.1	9.9
	CE (Kw·h)	312.84	0	0	312.84	312.84
Scheme 2	DGP (%)	73	0	0	73	73
	UDI (%)	60.16	60.49	50.92	-0.33	9.24
	CE (Kw·h)	263.54	0	0	263.54	263.54
Scheme 3	DGP (%)	1	0	0	1	1
	UDI (%)	56.75	62.51	50.92	-5.76	5.83
	CE (Kw·h)	227.87	0	0	227.87	227.87

Table 10. Scheme 2 metrics visualization comparison chart.

Different Integration Schemes	DGP Visualization	UDI Visualization
The solar-concentrating skin		<p data-bbox="802 725 1050 752">Useful daylight illuminance</p>
Common skin		<p data-bbox="802 1120 1050 1146">Useful daylight illuminance</p>
non-skin		<p data-bbox="802 1505 1050 1532">Useful daylight illuminance</p>

4. Discussion

4.1. Research Innovation

With the development of photovoltaic technology, the use of photovoltaic modules in buildings has become a way to use renewable energy; however, the integration of photovoltaic module forms with buildings can also affect the aesthetics of the building facade. Unlike previous studies that have addressed the integrated aesthetics of PV modules and the aesthetic potential of the modules [42,43], as well as the design of PV module geometries [16], this paper is more about optimizing the initial design through performance, starting from objective performance goals. The photovoltaic module used in this experiment was a transparent solar-concentrating-type module. Because it is transparent to operate, blocking the field of view less, it has a better visual experience perception than the CPV-T concentrating model and lens wall composite parabolic concentrating modules designed by Liang et al. [44] and Xuan et al. [45], and the shape is designed according to the adaptation window with a certain degree of aesthetics. In addition, compared with the study of Yi, Y,

K [35], this paper achieves a balanced optimization of the three objectives by considering the energy efficiency of solar concentrating as the optimization objective, while in the study of Xuan et al. [46], the energy efficiency, daylight objective, and the parabolic concentrating module are considered, while the parabolic concentrating module is placed in the skylight. However, this paper starts from the building façade, which can be directly perceived by human vision, and quantifies the performance index to explore the concentrating module and the integrated design with the building.

The simulation results show that the optimal tracking angle of the solar-concentrating module in this paper is in the range of 24° – 56° , which is smaller than the 20° – 70° proposed by Liang et al. [47]. However, the tracking type solar-concentrating modules used in this paper have certain advantages in vertical energy harvesting compared to the static solar-concentrating modules of Liu et al. [48] and Liang et al. [47]. Due to the absorption of direct light, the concentrating module can effectively reduce DGP by about 70% and improve UDI by about 10% compared to the nonmodule and common module, which improves the comfort of indoor light environment in general. Eltaweel et al. [49] used louvers to reflect sunlight into the room to improve indoor lighting and had over 90% of the indoor area can reach a UDI of 300–500 lux during working hours, unlike this paper, which can provide UDI in the range of 100–2000 lux for an average of 60% of the annual working hours; from Table 10, it can be calculated that 81% of the indoor area can achieve more than 60% of the time share., and the indoor year-round UDI level is at 58.71% (Table 5), which is lower than the low-frequency transmittance concentrating module designed by Zhang et al. [21] for the integration of light windows.

4.2. Limitations and Future Directions

Although the use of parametric methods for multiobjective optimization exhibit significant advantages, the accuracy and range of parameter settings still affect the distribution space of the optimized solution set. The calculated values of each design parameter in this experiment (Table 1) were chosen to take values in a decreasing form without a finer division, such as the number of solar-concentrating modules, based on one change, which would change the distribution of the solution set space based on two changes.

In addition, the solar-concentrating module is essentially a linear Fresnel lens, which is composed of tiny inscribed grooves that will change the light to achieve convergence of light; however, considering the simulation length of the experiment and the difficulty of constructing the inscribed grooves, this experiment equates the linear Fresnel lens into an ordinary glass with different transmittances; the projection and refraction of ordinary glass to change the light and inscribed grooves to change the light are somewhat different, which will have some impact on the experiment. The focus of the equivalence method was to calculate the transmittance. Because the luminous flux of the full wavelength band of the sun cannot be obtained in real time, the ratio of solar scattered radiation to total radiation was used as the approximate transmittance in this study, which has some deviation from the actual transmittance and will have an impact on the calculation accuracy. Therefore, the covariates should be further subdivided and the equivalence method should be changed in future studies to provide more accurate experimental results.

Based on the analysis of the optimization relationship between the dynamic concentrating skin design parameters and performance indices, this experiment provides a scheme and basic data for integrated design and constructs a multiobjective optimization workflow for solar-concentrating skin. In future work, we will optimize the solar-concentrating skin, design a more visually aesthetic skin, and explore the impact of skin on indoor light distribution.

5. Conclusions

This study uses Rhino Grasshopper as the parametric modeling platform and Ladybug, Honeybee, and Octopus as the performance analysis and data-processing platforms to demonstrate the entire modeling, simulation, and analysis process in detail. This study

helps to solve the multiobjective year-round conditions of the solar concentrating skin and constructs the technical framework of the entire process from the design optimization of the dynamic concentrating skin for the integrated design of solar energy technology and building to realize the closed-loop design.

The Pareto optimal solution set for multiobjective optimization of the solar-concentrating skin was organized, screened, and analyzed, and the optimization interval and optimal design interval of each design parameter were obtained. The conclusions are as follows:

1. The optimization interval of the number of solar-concentrating modules is between 15 and 17, and the best one is 17. The width optimization interval is 0.13 m–0.16 m, and the best is 0.16 m; the length optimization interval is 2.6 m–3.0 m, and the best is 3.0 m; the angle optimization is 25°–46°, and the best is 25°.
2. The correlation between DGP, UDI, and capacity efficiency is highly negative, and the correlation between UDI and capacity efficiency is moderately positive. When DGP is between 50% and 80%, UDI and CE decrease as DGP increases; when DGP is between 80% and 100%, CE decreases and then increases with DGP, and UDI increases and then decreases with DGP.
3. The correlation between each design parameter and the performance target is angle > width > amount > length.
4. By comparing the dynamic concentrating skin with the normal skin and the no-skin case, it was found that the dynamic concentrating skin can effectively reduce glare and increase the effective natural light level while achieving energy output. The daylight glare probability reduction rate can reach approximately 70% and the useful daylight illuminance can be increased by approximately 10%.

This study adopts a parametric performance simulation approach to explore how the high efficiency and capacity of solar-concentrating skins affect multiple performance targets in building interiors, and the relationship between concentrating skin design parameters and performance optimization. In addition, it provides multiple optimization integration schemes and an analytical simulation technical framework for the integration and optimization of dynamic concentrating skins in an effort to improve the building indoor light environment and reduce carbon emissions.

Author Contributions: Conceptualization, B.W. and Y.X.; data curation, Z.S., L.S., L.C. and C.C.; methodology, Z.S., B.W. and Y.X.; software, Z.S., B.W., L.S. and L.C.; validation, L.S., X.G. and L.C.; visualization, Z.S. and B.W.; writing—original draft, Z.S., B.W., Y.X., L.S. and C.C.; writing—review and editing, B.W., Y.X. and X.G. All authors have read and agreed to the published version of the manuscript.

Funding: This research was funded by the Fundamental Research Funds for the Central Universities, grant number 2020QN12.

Institutional Review Board Statement: Not applicable.

Informed Consent Statement: Not applicable.

Data Availability Statement: Data are available on request from the authors.

Conflicts of Interest: The authors declare no conflict of interest.

References

1. GlobalABC 2021 Global Status Report for Buildings and Construction. Available online: https://globalabc.org/sites/default/files/2021-10/GABC_Buildings-GSR-2021_BOOK.pdf (accessed on 6 November 2022).
2. Bian, M.; Zhang, X.; Yin, C.; Yang, L.; He, T.; Li, B.; Wang, M.; Wang, B.; He, Z. Research Status of Application Technology of Photovoltaic Modules on Building Facade. *Build. Sci.* **2020**, *36*, 127–135. (In Chinese) [[CrossRef](#)]
3. Irshad, K.; Habib, K.; Saidur, R.; Kareem, M.; Saha, B.B. Study of thermoelectric and photovoltaic facade system for energy efficient building development: A review. *J. Clean. Prod.* **2019**, *209*, 1376–1395. [[CrossRef](#)]
4. Zheng, J.; Sheng, G.; Cai, X.; Zhao, Y.; Xiao, X.; Xu, G. Recent Progress in Semi-Transparent Photovoltaic Devices and Their Applications. *Adv. NR Energy* **2021**, *9*, 461–478. [[CrossRef](#)]

5. Luo, T.; Yan, D.; Jiang, Y.; Zhao, J. Study on Lighting Energy Simulation Method for Office Buildings (Part I). *Build. Sci.* **2017**, *33*, 101–109. (In Chinese) [[CrossRef](#)]
6. Zhou, X.; Yan, D.; Hong, T.; Ren, X. Data analysis and stochastic modeling of lighting energy use in large office buildings in China. *Energy Build.* **2015**, *86*, 275–287. [[CrossRef](#)]
7. Zhu, L.; Shao, Z.; Sun, Y.; Soebarto, V.; Gao, F.; Zillante, G.; Zuo, J. Indoor daylight distribution in a room with integrated dynamic solar concentrating facade. *Energy Build.* **2018**, *158*, 1–13. [[CrossRef](#)]
8. Sun, Y.; Liu, D.; Flor, J.-F.; Shank, K.; Baig, H.; Wilson, R.; Liu, H.; Sundaram, S.; Mallick, T.K.; Wu, Y. Analysis of the daylight performance of window integrated photovoltaics systems. *Renew. Energy* **2020**, *145*, 153–163. [[CrossRef](#)]
9. Ullah, I. Fiber-based daylighting system using trough collector for uniform illumination. *Sol. Energy* **2020**, *196*, 484–493. [[CrossRef](#)]
10. Nick, N.; Anna, D.; Justin, S. Development of a Modeling Strategy for Adaptive Multifunctional Solar Energy Building Envelope Systems. Available online: <https://www.researchgate.net/publication/275214357> (accessed on 27 September 2022).
11. Zhu, L.; Chen, M.; Shao, Z.; Li, Q.; Sun, Y. Experimental and Simulation Study on Optical and Electrical Properties of Building Integrated 500×Solar Concentrating Photovoltaic Module. *Acta Energ. Sol. Sin.* **2021**, *42*, 247–252. (In Chinese) [[CrossRef](#)]
12. Anna, D.; Matt, G.; Peter, S.; Jason, V.; Nick, N.; Kenton, P.; Mohamed, A.; Brandon, A.; Satoshi, K. Next Generation High-Efficiency Solar Power Systems for Building Envelopes. Available online: <https://www.case.rpi.edu/research/icsolar> (accessed on 27 September 2022).
13. Novelli, N.; Phillips, K.; Shultz, J.; Derby, M.M.; Salvat, R.; Craft, J.; Stark, P.; Jensen, M.; Derby, S.; Dyson, A. Experimental investigation of a building-integrated, transparent, concentrating photovoltaic and thermal collector. *Renew. Energy* **2021**, *176*, 617–634. [[CrossRef](#)]
14. Chemisana, D. Building integrated concentrating photovoltaics: A review. *Renew. Sustain. Energy Rev.* **2011**, *15*, 603–611. [[CrossRef](#)]
15. Maghrabie, H.M.; Elsaid, K.; Sayed, E.T.; Abdelkareem, M.A.; Wilberforce, T.; Olabi, A. Building-integrated photovoltaic/thermal (BIPVT) systems: Applications and challenges. *Sustain. Energy Technol. Assess.* **2021**, *45*, 101151. [[CrossRef](#)]
16. Parupudi, R.V.; Singh, H.; Kolokotroni, M. Low Concentrating Photovoltaics (LCPV) for buildings and their performance analyses. *Appl. Energy* **2020**, *279*, 115839. [[CrossRef](#)]
17. Baig, H.; Chemisana, D.; Sundaram, S.; Mallick, T. Conjugate refractive–reflective based building integrated photovoltaic system. *Mater. Lett.* **2018**, *228*, 25–28. [[CrossRef](#)]
18. Hong, M.; Feng, C.; Xu, Z.; Zhang, L.; Zheng, H.; Wu, G. Performance study of a new type of transmissive concentrating system for solar photovoltaic glass curtain wall. *Energy Convers. Manag.* **2019**, *201*, 112167. [[CrossRef](#)]
19. Xuan, Q.; Li, G.; Lu, Y.; Zhao, B.; Zhao, X.; Su, Y.; Ji, J.; Pei, G. Design, optimization and performance analysis of an asymmetric concentrator-PV type window for the building south wall application. *Sol. Energy* **2019**, *193*, 422–433. [[CrossRef](#)]
20. Xuan, Q.; Li, G.; Lu, Y.; Zhao, B.; Wang, F.; Pei, G. Daylighting utilization and uniformity comparison for a concentrator-photovoltaic window in energy saving application on the building. *Energy* **2021**, *214*, 118932. [[CrossRef](#)]
21. Zhang, W.; Li, J.; Xie, L.; Hao, X.; Mallick, T.; Wu, Y.; Baig, H.; Shanks, K.; Sun, Y.; Yan, X. Comprehensive analysis of electrical-optical performance and application potential for 3D concentrating photovoltaic window. *Renew. Energy* **2022**, *189*, 369–382. [[CrossRef](#)]
22. Eltaweel, A.; Yuehong, S. Using integrated parametric control to achieve better daylighting uniformity in an office room: A multi-Step comparison study. *Energy Build.* **2017**, *152*, 137–148. [[CrossRef](#)]
23. Rashwan, A.; El Gizawi, L.; Sheta, S. Evaluation of the effect of integrating building envelopes with parametric patterns on daylighting performance in office spaces in hot-dry climate. *Alex. Eng. J.* **2019**, *58*, 551–557. [[CrossRef](#)]
24. Kim, H.; Clayton, M.J. A multi-objective optimization approach for climate-adaptive building envelope design using parametric behavior maps. *Build. Environ.* **2020**, *185*, 107292. [[CrossRef](#)]
25. Salimzadeh, N.; Vahdatikhaki, F.; Hammad, A. Parametric modeling and surface-specific sensitivity analysis of PV module layout on building skin using BIM. *Energy Build.* **2020**, *216*, 109953. [[CrossRef](#)]
26. Bahdad, A.; Fadzil, S.; Onubi, H.; BenLasod, S. Multi-dimensions optimization for optimum modifications of light-shelves parameters for daylighting and energy efficiency. *Int. J. Environ. Sci. Technol.* **2022**, *19*, 2659–2676. [[CrossRef](#)]
27. Hu, J.; Wang, Z.; Chen, W. *A Study on Automatic Form Optimization Procedures of Building Performance Design Based on “Ladybug+Honeybee”*; IOP Conference Series: Earth Environment Science; IOP Publishing: Bristol, UK, 2020; p. 012020. [[CrossRef](#)]
28. Kharvari, F. An empirical validation of daylighting tools: Assessing radiance parameters and simulation settings in Ladybug and Honeybee against field measurements. *Sol. Energy* **2020**, *207*, 1021–1036. [[CrossRef](#)]
29. Fang, Y.; Cho, S. Design optimization of building geometry and fenestration for daylighting and energy performance. *Sol. Energy* **2019**, *191*, 7–18. [[CrossRef](#)]
30. Sun, C.; Liu, Q.; Han, Y. Many-objective optimization design of a public building for energy, daylighting and cost performance improvement. *Appl. Sci.* **2020**, *10*, 2435. [[CrossRef](#)]
31. Toutou, A.; Fikry, M.; Mohamed, W. The parametric based optimization framework daylighting and energy performance in residential buildings in hot arid zone. *Alex. Eng. J.* **2018**, *57*, 3595–3608. [[CrossRef](#)]
32. Fan, Z.; Liu, M.; Tang, S. A multi-objective optimization design method for gymnasium facade shading ratio integrating energy load and daylight comfort. *Build. Environ.* **2022**, *207*, 108527. [[CrossRef](#)]

33. Mahdavejad, M.; Nazar, N.S. Daylightophil high-performance architecture: Multi-objective optimization of energy efficiency and daylight availability in BSk climate. *Energy Procedia* **2017**, *115*, 92–101. [[CrossRef](#)]
34. Zhang, A.; Bokel, R.; van den Dobbelsteen, A.; Sun, Y.; Huang, Q.; Zhang, Q. Optimization of thermal and daylight performance of school buildings based on a multi-objective genetic algorithm in the cold climate of China. *Energy Build.* **2017**, *139*, 371–384. [[CrossRef](#)]
35. Yi, Y.K. Building facade multi-objective optimization for daylight and aesthetical perception. *Build. Environ.* **2019**, *156*, 178–190. [[CrossRef](#)]
36. Zomorodian, Z.S.; Tahsildoost, M. Assessing the effectiveness of dynamic metrics in predicting daylight availability and visual comfort in classrooms. *Renew. Energy* **2019**, *134*, 669–680. [[CrossRef](#)]
37. Nabil, A.; Mardaljevic, J. Useful daylight illuminances: A replacement for daylight factors. *Energy Build.* **2006**, *38*, 905–913. [[CrossRef](#)]
38. Wienold, J.; Christoffersen, J. Evaluation methods and development of a new glare prediction model for daylight environments with the use of CCD cameras. *Energy Build.* **2006**, *38*, 743–757. [[CrossRef](#)]
39. Wu, W.; Liu, K. An Introduction of New Daylighting Evaluation Criteria: A Replacement for Daylight Factor. Nanjing. *China Illum. Eng. J.* **2012**, *23*, 1–7+24. [[CrossRef](#)]
40. Wienold, J. Dynamic Daylight Glare Evaluation. In Proceedings of the Building Simulation, Eleventh International IBPSA Conference, Glasgow, Scotland, 27–30 July 2009; Available online: http://ibpsa.org/proceedings/BS2009/BS09_0944_951.pdf (accessed on 6 November 2022).
41. Laboratory, N.R.E. Weather Data by Location, Asia WMO Region 2-Chin. Available online: https://energyplus.net/weather-location/asia_wmo_region_2/CHN/CHN_Jiangsu.Xuzhou.580270_CSWD (accessed on 6 November 2022).
42. Kim, S.K.; Lee, K.S. A Study on the Aesthetic Elements for Building Integrated Photovoltaics (BIPV) Design. *J. Archit. Inst. Korea* **2021**, *37*, 53–64. [[CrossRef](#)]
43. Foo, A.Y.; Saw, M.H.; Khoo, Y.S.; Tay, S.E.R. Developing a Methodology towards Designing Aesthetical BIPV Modules. In Proceedings of the IEEE 48th Photovoltaic Specialists Conference (PVSC), Fort Lauderdale, FL, USA, 20–25 June 2021; pp. 0272–0277.
44. Liang, S.; Zheng, H.; Wang, X.; Ma, X.; Zhao, Z. Design and performance validation on a solar louver with concentrating-photovoltaic-thermal modules. *Renew. Energy* **2022**, *191*, 71–83. [[CrossRef](#)]
45. Xuan, Q.; Li, G.; Jiang, B.; Zhao, X.; Zhao, B.; Ji, J.; Pei, G. Analysis and quantification of effects of the diffuse solar irradiance on the daylighting performance of the concentrating photovoltaic/daylighting system. *Build. Environ.* **2021**, *193*, 107654. [[CrossRef](#)]
46. Xuan, Q.; Li, G.; Zhao, B.; Jiang, B.; Sun, D.; Zhang, X.; Tang, J.; Zhuang, Y.; Liu, J.; Li, L. Evaluation of the smart daylighting control performance of the concentrating photovoltaic/daylighting system as the skylight in the building. *Sol. Energy* **2022**, *238*, 17–29. [[CrossRef](#)]
47. Liang, S.; Zheng, H.; Liu, S.; Ma, X. Optical design and validation of a solar concentrating photovoltaic-thermal (CPV-T) module for building louvers. *Energy* **2022**, *239*, 122256. [[CrossRef](#)]
48. Liu, X.; Wu, Y. Design, development and characterisation of a Building Integrated Concentrating Photovoltaic (BICPV) smart window system. *Sol. Energy* **2021**, *220*, 722–734. [[CrossRef](#)]
49. Eltaweel, A.; Su, Y.; Lv, Q.; Lv, H. Advanced parametric louver systems with bi-axis and two-layer designs for an extensive daylighting coverage in a deep-plan office room. *Sol. Energy* **2020**, *206*, 596–613. [[CrossRef](#)]